Vapor-liquid equilibrium and critical behavior of the square-well fluid of variable range: A theoretical study

Elisabeth Schöll-Paschinger[a)]
Fakultät für Physik, Universität Wien, Boltzmanngasse 5, A-1090 Wien, Austria

Ana Laura Benavides and Ramon Castañeda-Priego
Instituto de Física, Universidad de Guanajuato, Lomas del Campestre 103, Lomas del Bosque, 37150, León, México

(Received 13 September 2005; accepted 18 October 2005; published online 22 December 2005)

The vapor-liquid phase behavior and the critical behavior of the square-well (SW) fluid are investigated as a function of the interaction range, $\lambda \in [1.25, 3]$, by means of the self-consistent Ornstein-Zernike approximation (SCOZA) and analytical equations of state based on a perturbation theory [A. L. Benavides and F. del Rio, Mol. Phys. **68**, 983 (1989); A. Gil-Villegas, F. del Rio, and A. L. Benavides, Fluid Phase Equilib. **119**, 97 (1996)]. For this purpose the SCOZA, which has been restricted up to now to a few model systems, has been generalized to hard-core systems with arbitrary interaction potentials requiring a fully numerical solution of an integro-partial differential equation. Both approaches, in general, describe well the liquid-vapor phase diagram of the square-well fluid when compared with simulation data. SCOZA yields very precise predictions for the coexistence curves in the case of long ranged SW interaction ($\lambda > 1.5$), and the perturbation theory is able to predict the binodal curves and the saturated pressures, for all interaction ranges considered if one stays away from the critical region. In all cases, the SCOZA gives very good predictions for the critical temperatures and the critical pressures, while the perturbation theory approach tends to slightly overestimate these quantities. Furthermore, we propose analytical expressions for the critical temperatures and pressures as a function of the square-well range.
 [DOI: 10.1063/1.2137713]

I. INTRODUCTION

In the last decades the square-well (SW) fluid has been the subject of extensive studies using different statistical mechanical methods. This is due to the following reasons: On the one hand, the SW fluid itself represents a good and simple model that includes the presence of attractive and repulsive forces and is able to reproduce the behavior of simple fluids. On the other hand, it has been incorporated as an important ingredient in theories for complex fluids, including mixtures, chain molecules, associating fluids, and polar fluids, among others. Reference 1 gives an idea of the state of the art of the methods and applications explored with the SW potential. Furthermore, different values of the interaction range cover a large variety of different systems ranging from sticky hard spheres in the limiting case of infinitely deep and infinitely short-ranged SW potentials to the van der Waals limit for long-ranged and very shallow potentials. Recently, renewed attention has been paid to short-ranged SW fluids[2–5] as a model of colloids and protein solutions.[6,7]

Due to advanced simulation techniques and sophisticated integral equation and perturbation theories, the liquid-vapor phase diagram of the SW fluid is now very well understood.[1,8,9] As a consequence, there are nowadays several analytic equations of state available for different values of the range of the potential.[2,3,10–16] Here, we have selected two theoretical methods and investigate their accuracy by comparison with available simulation data for intermediate and long ranges $\lambda \in [1.25, 3]$: the self-consistent Ornstein-Zernike approach (SCOZA) and a perturbation theory. In particular, we test their reliability when being applied to the determination of the vapor-liquid transition.

The first theoretical approach used in this work is the SCOZA, an advanced self-consistent integral equation theory that has been applied with success to a variety of Hamiltonian systems: discrete systems such as the lattice gas[17] as well as continuum systems such as the Yukawa fluid.[18] It is based on a generalized mean-spherical ansatz (MSA), introducing in the MSA closure relation a state-dependent function that is fixed through a thermodynamic consistency criterion. Comparison with computer simulations showed in an impressive way that SCOZA yields globally accurate structural and thermodynamic properties even near the phase transitions and in the critical region. Recently, it has also been generalized to the study of binary mixtures.[19,20] The only drawback of the method is its restriction to model systems for which the MSA is semianalytically solvable, like the Yukawa[18] or the Sogami-Ise fluid.[21] A major challenge is thus the solution of the SCOZA equations when one goes beyond linear combinations of Yukawa tails that model the soft contributions of the pair potential. This is done in this work: we present here the generalization of the SCOZA to hard-core potentials with arbitrary tails and describe the nu-

a)Electronic mail: elisabeth.schoell-paschinger@univie.ac.at

merical solution algorithm of the SCOZA integro-partial differential equation. In particular, we present its application to the SW potential.

The second theoretical approach considers the intermediate-range square-well equation of state (IRSWEOS) developed by Gil-Villegas *et al.*[16] for $1.25<\lambda \leqslant 2$ and the long-range square-well equation of state (LRSWEOS) for $\lambda>2$ obtained by Benavides and del Río.[15] Both equations were developed by using a perturbation theory. They are analytical in the temperature, density, and intermolecular parameters. These equations have been incorporated in perturbation theories for discrete potentials,[22] polar square-well fluids,[23–26] and binary mixtures.[27] At the time they were obtained they were compared with available simulation data, but since more refined simulation techniques have been developed recently, we will actualize the comparison in this work. In particular, we compare the LRSWEOS with recent simulation data for $2<\lambda<3$[10]. To the best of our knowledge this region had never been investigated by simulation techniques before, and this is the first time that the long-range equation of state proposed by Benavides and del Río will be tested.[15] For the case of the longest interaction range $\lambda=3$ this equation reproduces very well the simulation data.[9,28]

In Sec. II we describe the SCOZA method and the analytical equations of state used in the present work. The SW phase diagrams, the saturation pressures, and the critical points for different interaction ranges are shown and discussed in Sec. III. Comparisons with available simulation data are included and particular emphasis is put on the critical region. Finally, in Sec. IV we close our paper with some conclusions and perspectives.

II. THEORETICAL APPROACHES

We consider a system of spherical particles of diameter σ which are interacting via a square-well potential ϕ_{SW} given by

$$\phi_{\mathrm{SW}}(r)=\begin{cases}\infty & r<\sigma\\ -\epsilon & \sigma\leqslant r\leqslant\lambda\sigma\\ 0 & r>\lambda\sigma,\end{cases} \tag{1}$$

where r is the interparticle distance, ϵ is the depth of the potential, and λ is the reduced range of the potential well. Appropriate reduced quantities can be defined by scaling with the energy depth ϵ and the hard-core diameter σ, e.g., $T^*=kT/\epsilon$, $\rho^*=\rho\sigma^3$. The two approaches used in this work are presented in the following.

A. SCOZA for arbitrary hard-core potentials

The self-consistent Ornstein-Zernike approximation (SCOZA) is based on a generalized MSA, introducing in the MSA relation one or more density- and temperature-dependent functions which are determined by enforcing consistency between two or three different routes to thermodynamics. Although the first concepts of SCOZA were proposed by Høye and Stell[29,30] nearly 30 years ago, its numerical solution remained for a long time an unsolved problem and its practical applications started only in 1996.[17] Up to now SCOZA has been solved for a small number of discrete systems,[17,31–36] and continuum systems,[19,20,37–41] and the results showed—when compared with computer simulations—that the theory gives very accurate predictions for the coexistence curves, even in the critical region, where conventional liquid-state theories usually have to face the following problems: the shape of the coexistence curve and the location of the critical point are not reproduced correctly, and the critical exponents are not the exact ones. Some theoretical approaches even fail to converge in the critical region, so that the liquid and vapor branches of the coexistence curve remain unconnected. SCOZA is able to cope with these problems: the liquid-vapor coexistence curve and the critical point are localized very accurately, and the critical exponents that have been studied both analytically by Høye *et al.*[42] and numerically by investigating the effective exponents[18,31,32] are close to the exact ones. However, in the case of continuum fluids, applications of the SCOZA have been restricted up to now to hard-core interactions with a formally arbitrary number of adjacent Yukawa[18] or Sogami-Ise[21] tails since the SCOZA formulation largely takes advantage of the availability of the semianalytic MSA solution for these systems. In order to solve SCOZA for other pair potentials such as the Lennard-Jones[38] or the Girifalco potential for fullerenes,[40] these had to be approximated by linear combinations of Yukawa tails. The obvious success of the SCOZA has motivated us to contribute to its extension: here, we present the—now fully numerical—solution of SCOZA for an arbitrary hard-core potential $\phi(r)$ given by

$$\phi(r)=\begin{cases}\infty & r\leqslant\sigma\\ w(r) & r>\sigma,\end{cases} \tag{2}$$

where the repulsion is characterized by the hard-sphere diameter σ and $w(r)$ is an arbitrary tail. As will be shown in the following the solution of the SCOZA for an arbitrary hard-core potential corresponds to the solution of an integro-partial differential equation.

The version of the SCOZA considered here is based on the Ornstein-Zernike (OZ) equation

$$h(r)=c(r)+\rho\int d^3r'c(r')h(|r-r'|) \tag{3}$$

supplemented with the following closure relation:

$$g(r)=0 \quad \text{for } r\leqslant\sigma,$$

$$c(r)=c_{\mathrm{HS}}(r)+K(\rho,\beta)w(r) \quad \text{for } r>\sigma. \tag{4}$$

$h(r)$ and $c(r)$ are the total and direct correlation functions; $g(r)=h(r)-1$ is the pair distribution function; $c_{\mathrm{HS}}(r)$ is the direct correlation function of the hard-sphere (HS) reference system given, for example, by the Waisman parametrization;[43] and $K(\rho,\beta)$ is a yet undetermined function depending on the thermodynamic state that is given by the density ρ and the inverse temperature $\beta=1/k_BT$, k_B being the Boltzmann constant. The closure resembles the one used in the lowest-order gamma-ordered (LOGA) approximation, which is equivalent to the optimized random-phase approximation[44,45] (ORPA) where $K(\rho,\beta)=-\beta$ is fixed.

Here, $K(\rho,\beta)$ is not given *a priori* but is determined through the thermodynamic self-consistency requirement between the compressibility and the energy route to the thermodynamic properties.[46]

We recall that, according to the compressibility route, the reduced isothermal compressibility is given by

$$\frac{1}{\chi^{\mathrm{red}}} = \frac{\partial \beta P}{\partial \rho} = 1 - \rho \tilde{c}(k=0), \tag{5}$$

where $\tilde{c}(k)$ denotes the Fourier transform of $c(r)$

$$\tilde{c}(k) = \int c(r) e^{-i\mathbf{kr}}\, d^3 r. \tag{6}$$

On the other hand, the excess (over ideal) internal energy per unit volume u, calculated via the internal energy route, is

$$\frac{U^{\mathrm{ex}}}{V} = u = 2\pi\rho^2 \int_\sigma^\infty dr\, r^2 w(r) g(r). \tag{7}$$

If χ^{red} and u are consistent with each other, they must stem from a unique Helmholtz free-energy density $F/V=f=f^{\mathrm{id}}+f^{\mathrm{ex}}$, where f^{id} and f^{ex} are the ideal and excess parts of the free-energy density. Thus

$$\rho \frac{\partial^2 u}{\partial \rho^2} = \rho \frac{\partial^2}{\partial \rho^2} \frac{\partial \beta f^{\mathrm{ex}}}{\partial \beta} = \frac{\partial}{\partial \beta}\left(\rho \frac{\partial \beta \mu^{\mathrm{ex}}}{\partial \rho} \right) = \frac{\partial}{\partial \beta}\left(\frac{1}{\chi^{\mathrm{red}}} \right), \tag{8}$$

where $\mu^{\mathrm{ex}} = \partial f^{\mathrm{ex}}/\partial \rho$ is the excess chemical potential. For approximate $g(r)$ (as obtained, for instance, by conventional integral equation and perturbation theories[46]) Eq. (8), where χ^{red} is given by Eq. (5) and u by Eq. (7), is not fulfilled. In the SCOZA, however, this consistency is enforced through an appropriate choice of the yet undetermined function $K(\rho,\beta)$ that is obtained by solving the partial differential equation (PDE) [Eq. (8)] supplemented by Eqs. (3), (4), (5), and (7).

First, we reformulate the PDE [Eq. (8)] as a PDE for the unknown function u

$$\rho \frac{\partial^2 u}{\partial \rho^2} = \frac{\partial}{\partial u}\left(\frac{1}{\chi^{\mathrm{red}}} \right) \frac{\partial u}{\partial \beta} = B(\rho,u) \frac{\partial u}{\partial \beta}, \tag{9}$$

where the diffusion coefficient of the quasilinear diffusion equation is $B(\rho,\beta) = \partial/\partial u (1/\chi^{\mathrm{red}})$. In the numerical solution of the PDE the partial derivative $\partial/\partial u (1/\chi^{\mathrm{red}})$ is approximated by the central difference quotient

$$\frac{\partial}{\partial u}\left(\frac{1}{\chi^{\mathrm{red}}} \right)(\rho,u) \sim \left(\frac{1}{\chi^{\mathrm{red}}}(\rho,u+\Delta u) - \frac{1}{\chi^{\mathrm{red}}}(\rho,u-\Delta u) \right) \Big/ (2\Delta u). \tag{10}$$

What remains is to determine χ^{red} as a function of u. This will be outlined in the following: First, we determine the unknown function $K(\rho,\beta)$ for a given value of u by solving the nonlinear equation

$$F(\rho,K,u) = u - 2\pi\rho^2 \int_\sigma^\infty dr r^2 w(r) g(r;K) = 0, \tag{11}$$

with the Newton-Raphson (NR) method (the derivative required in this scheme is approximated numerically). In each step of the NR iteration the pair distribution function $g(r;K)$ is determined for a given value of K by solving the OZ equation (3) together with the closure relation (4) using the Labik, Malijevsky, and Vonka (LMV) algorithm,[47] which is a powerful combination of a Newton-Raphson technique and a Picard iteration. Once K is determined for a given value of u it is straightforward to calculate the direct correlation function $c(r;u)$ and thus $\chi^{\mathrm{red}}(\rho,u)$ from Eq. (5).

The PDE has been solved numerically via an implicit finite-difference algorithm described in detail in[31] in the region $(\beta,\rho) \in [0,\beta_f] \times [0,\rho_0]$. The integration with respect to β starts at $\beta=0$ and goes down to lower temperatures. At each density and temperature the nonlinear equation $F(\rho,K,u)=0$ is solved, yielding K and thus χ^{red} for a given value of $u+\Delta u$ and $u-\Delta u$. To ensure rapid convergence of the NR iteration we take as initial guess for the values of K the solution at the previous temperature step.

The boundary conditions are the following: For $\rho=0$ we set

$$u(\rho=0,\beta) = 0, \quad \forall\, \beta. \tag{12}$$

For the boundary condition at high density ρ_0 we make use of the so-called high-temperature approximation

$$\frac{\partial^2 u}{\partial \rho^2}(\rho_0,\beta) = \frac{\partial^2 u}{\partial \rho^2}(\rho_0,\beta=0), \quad \forall\, \beta. \tag{13}$$

The initial condition $u(\rho,\beta=0)$ can be determined by taking into account that for $\beta=0$ the direct correlation function $c(r)$ coincides with that of the HS gas, thus $K(\rho,\beta=0)=0$. The unphysical region inside the spinodal is excluded from the integration, and the boundary conditions on the spinodal are chosen as follows: the value of K on the spinodal is obtained by solving numerically the nonlinear equation

$$F(\rho,K) = \frac{1}{\chi^{\mathrm{red}}} = 1 - \rho \bar{c}(k=0,K) = 0 \tag{14}$$

via a NR technique. In each step of the NR iteration $\bar{c}(k=0,K)$ is determined by solving Eq. (3) supplemented with (4). Once we have K, and thus the structure functions, the internal energy on the spinodal u_S is calculated from the energy route Eq. (7) and the boundary conditions on the spinodal are

$$u(\rho_{S_i},\beta) = u_S(\rho_{S_i}), \quad i=1,2, \tag{15}$$

where $\rho_{S_i}(i=1,2)$ are approximations of the spinodal densities on the discrete density grid at a given temperature. Their values are determined by locating the change of sign of $1/\chi^{\mathrm{red}}$.

Once $u(\rho,\beta)$ has been calculated by solving the PDE (9), the pressure P and the chemical potential μ are obtained by integrating $\partial \beta P/\partial \beta$ and $\partial \beta \mu/\partial \beta$

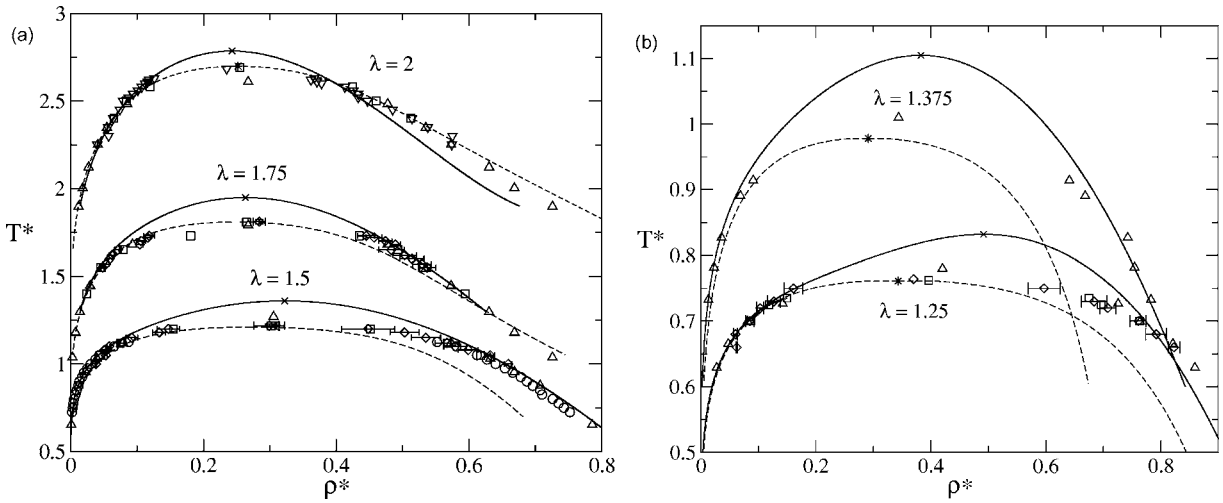

FIG. 1. (a) Liquid-vapor phase diagram of a SW fluid of intermediate range $\lambda=2$, 1.75, and 1.5 in the (T^*,ρ^*) plane. The solid and dashed lines represent the IRSWEOS and the SCOZA results, respectively. Symbols show the simulation data of del Río *et al.* (□) (Ref. 1), Elliot and Hu (△) (Ref. 51), Patel *et al.* (○) (Ref. 10), Vega *et al.* (◇) (Ref. 52), and de Miguel (▽) (Ref. 53). We also show the critical points predicted by IRSWEOS (×) and SCOZA (★). (b) Liquid-vapor phase diagram of a SW fluid of intermediate range $\lambda=1.375$ and 1.25 in the (T^*,ρ^*) plane. The solid and dashed lines represent IRSWEOS and SCOZA results, respectively. Symbols show the simulation data of del Río *et al.* (□) (Ref. 1), Elliot and Hu (△) (Ref. 51), and Vega *et al.* (◇) (Ref. 52). We also show the critical points predicted by IRSWEOS (×) and SCOZA (★).

$$\frac{\partial \beta P}{\partial \beta} = -u + \rho \frac{\partial u}{\partial \rho}, \tag{16}$$

$$\frac{\partial \beta \mu}{\partial \beta} = \frac{\partial u}{\partial \rho}, \tag{17}$$

with respect to β, where we have taken as integration constants at $\beta=0$ the Carnahan-Starling[48] values for βP and $\beta\mu$

$$\beta P(\rho,\beta=0) = \rho \frac{1+\eta+\eta^2-\eta^3}{(1-\eta)^3},$$

$$\beta \mu(\rho,\beta=0) = \ln \rho + \frac{8\eta - 9\eta^2 - 3\eta^3}{(1-\eta)^3}, \tag{18}$$

where $\eta=\rho\sigma^3\pi/6$ is the packing fraction.

For the numerical solution of the PDE we have chosen a density and temperature grid spacing of $\Delta\rho^*=\Delta\rho\sigma^3=0.001$ and $\Delta\beta^*=\epsilon\Delta\beta=5\times10^{-4}$ for $\lambda>1.5$ and $\Delta\beta=5\times10^{-3}$ for $\lambda\leqslant1.5$. Furthermore we have used $\rho_0^*=1.2$ for $\lambda>1.5$ and $\rho_0^*=1.15$ for $\lambda\leqslant1.5$ and $\Delta u^*=\Delta u\sigma^3/\epsilon=10^{-4}$. For the Fourier transforms required in the LMV algorithm we have used for the discrete representation of the structure functions 1024 grid points with a spacing of $\Delta r^*=\Delta r/\sigma=0.01$ in real space.

B. Perturbation theory

We have selected the intermediate-range square-well equation of state (IRSWEOS) developed by Gil-Villegas *et al.*[16] for $1.25<\lambda<2$ and the long-range square-well equation of state (LRSWEOS) for $\lambda\geqslant2$ obtained by Benavides and del Río[15] since they describe very well the SW thermodynamic properties in a wide range of temperatures and densities. Both equations have been obtained from the high-temperature perturbation expansion, originally introduced by Barker and Henderson.[49] In this approach the excess Helmholtz free energy can be expressed as

$$\frac{A}{NkT} = \frac{A^{\mathrm{HS}}}{NkT} + \frac{1}{T^*}a_1(\rho^*,\lambda) + \frac{1}{T^{*2}}a_2(\rho^*,\lambda) + a_R(\rho^*,\lambda,T^*), \tag{19}$$

where A_{HS} is the free energy of the hard-sphere reference fluid; $a_1(\rho^*,\lambda), a_2(\rho^*,\lambda)$, and $a_R(\rho^*,\lambda,T^*)$ are the first-order, second-order, and residual perturbation terms, respectively; and $T^*=k_BT/\epsilon$ is the reduced temperature. For the IRSWEOS, the explicit analytical expressions for these terms are given in Ref. 16. The residual term is an estimate of the higher-order terms. The LRSWEOS is a second-order theory which means that there is no residual term. The explicit form of $a_1(\rho^*,\lambda)$ and $a_2(\rho^*,\lambda)$ can be found in Ref. 15. The main advantage of this equation of state is that it provides a correction to the van der Waals limit and that its low-density expansion is exact to the order of the fourth virial coefficient. The second-order terms of both equations of state are more accurate than the corresponding local compressibility approximation (LCA) or macroscopic compressibility approximation (MCA) values proposed by Barker and Henderson.[49] Both equations give results that are comparable to those produced by the equation of state proposed by Patel *et al.*[10]

III. LIQUID-VAPOR PHASE DIAGRAM AND CRITICAL BEHAVIOR FOR VARIABLE INTERACTION RANGE

One way to test the theoretical approaches used in this work is to analyze the vapor-liquid phase diagrams predicted by both frameworks and compare them with available simulation data.[50] Special attention is devoted to the critical region where SCOZA is known to yield accurate results. In this analysis we have considered two regimes of λ values: intermediate $(1.25\leqslant\lambda\leqslant2)$ and long $(2<\lambda\leqslant3)$ ranges.

In Figs. 1(a) and 1(b) the liquid-vapor phase diagram of a SW fluid of intermediate range λ is shown. In this and in

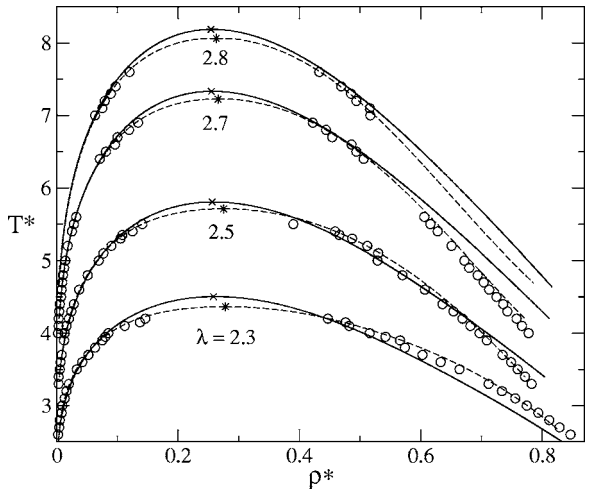

FIG. 2. Liquid-vapor phase diagram of a SW fluid of long range $\lambda=2.3$, 2.5, 2.7, and 2.8. The solid and dashed lines represent the LRSWEOS and SCOZA results, respectively. We also show the critical points (CP) predicted by both LRSWEOS (×) and SCOZA (★). No simulation data are available for the CP in this λ regime. Open circles show the simulation data of Patel *et al.* (○) (Ref. 10).

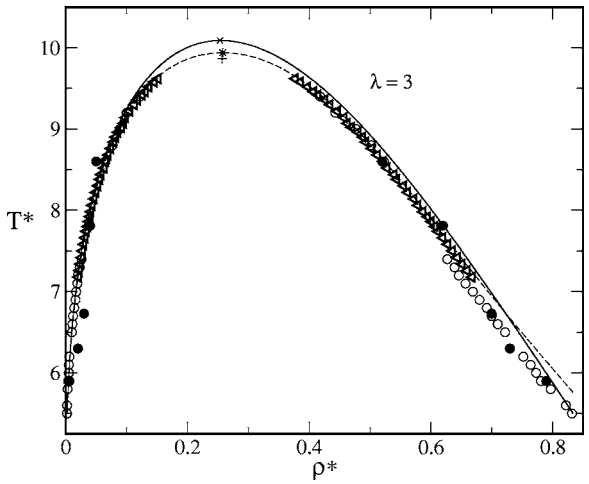

FIG. 3. Liquid-vapor phase diagram of a SW fluid for $\lambda=3$. The solid and dashed lines represent the LRSWEOS and the SCOZA results, respectively. We also show the critical points predicted by LRSWEOS (×), SCOZA (★), and Orkoulas and Panagiotopoulos (+) (Ref. 9). Symbols show the simulation data of Benavides *et al.* (●) (Ref. 28), Orkoulas and Panagiotopoulos (◁), and Patel *et al.* (○) (Ref. 10).

the following figures, the solid and dashed lines represent the perturbation equations of state (IRSWEOS and LRSWEOS) and the SCOZA results, respectively. Symbols show the simulation data obtained by del Río *et al.*[1] via a hybrid Monte Carlo method, by Elliott and Hu[51] using molecular-dynamics simulations, by Patel *et al.*[10] who performed both Gibbs ensemble Monte Carlo (GEMC) and *NVT*-Monte Carlo simulations, by Vega *et al.*[52] with Gibbs Ensemble Monte Carlo, and by de Miguel[53] who used finite-size scaling techniques to explore the critical region. As we can see, both theoretical approaches give quantitatively good agreement with the simulation data, specially for the vapor side of the coexistence line. For higher coexistence densities and for $\lambda\leqslant 1.5$ the IRSWEOS gives better predictions than SCOZA if one stays away from the critical region, while for $\lambda=2$ and high saturated densities, the agreement of SCOZA with simulation data is better than that of the IRSWEOS. As expected, the IRSWEOS overestimates the critical points and SCOZA gives very good predictions for all the λ values considered.

In Fig. 2 we show the liquid-vapor phase diagram for $2<\lambda<3$. Both approaches are in good agreement with the simulation data by Patel *et al.*[10] It seems that the SCOZA predictions are more accurate than the LRSWEOS. However, in the region $0.4<\rho^*<0.6$ and for λ values of 2.3, 2.5, and 2.7, the simulation data vary in a discontinuous way when switching from *NVT* results to GEMC results; some data are reproduced well by SCOZA and others by LRSWEOS (see also Fig. 3). This behavior seems to be due to the use of Gibbs ensemble and *NVT* simulation techniques for the different regions of temperature. Unfortunately, Patel *et al.* have not reported the correct uncertainties on their simulated data,[54] and the size of the symbols that we selected is not necessarily a real estimation of the errors. Since no simulation data are available for the critical points, we show in Fig. 2 only the critical points predicted by both LRSWEOS and SCOZA.

Both theories show good agreement at the highest λ value considered in this work although LRSWEOS overestimates the critical temperature, as we can see directly from Fig. 3. In this figure we compare our results with three independent sets of simulation data calculated with different techniques: Benavides *et al.*[28] who used the molecular-dynamics technique, Orkoulas and Panagiotopoulos who performed grand canonical Monte Carlo (GCMC) simulations,[9] and Patel *et al.*[10] who performed both GEMC and *NVT*-Monte Carlo simulations. We notice that far from the critical region the main differences between the theoretical approaches and simulation data appear for high coexistence densities and reduced temperatures below 7.5. As in Fig. 2, simulation data show different tendencies. Then still, the origin of the discrepancies between our theoretical results and simulation data is not clear. Additionally, more simulation studies would be required.

Figure 4 shows the reduced critical temperature T_c^* as a function of the SW range. Both theories predict very well the tendency of the reduced critical temperatures. We notice that the IRSWEOS and LRSWEOS overestimate the T_c^* systematically. If we consider that SCOZA predicts the critical points with high accuracy, as becomes visible in the phase diagrams of Figs. 1–3, the SCOZA results for the different λ values considered in this work can be used as a good prediction of the critical temperatures. This allows us to propose the following analytical expression for the reduced critical temperature as a function of the interaction range λ that was obtained by a polynomial fit to the SCOZA predictions: $T_c^*(\lambda)=3.737-5.172\lambda+2.205\lambda^2+0.070\lambda^3$.

The reduced critical density ρ_c^* as a function of λ is shown in Fig. 5. A clear dispersion of the simulation data predicted by several authors can be seen, making a comparison with the theories presented here rather difficult. Nevertheless, both theoretical approaches follow qualitatively the behavior of the reduced critical densities shown separately for each author (see, for example, the results indicated by the

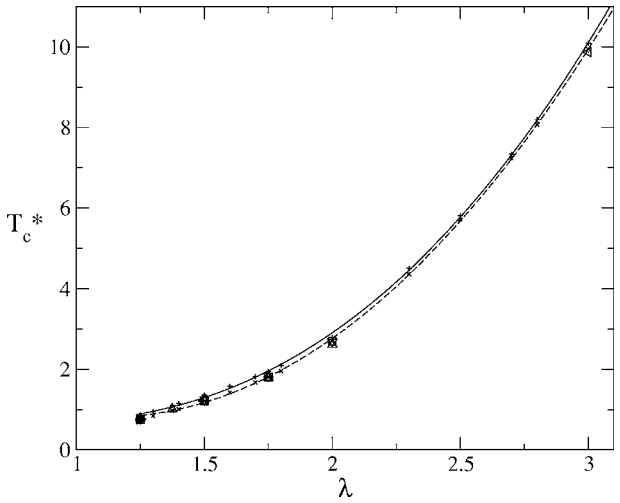

FIG. 4. Critical temperature as a function of the range of the potential, λ. The solid and dashed lines are a polynomial fit to the critical temperatures predicted by both perturbation theory (IRSWEOS and LRSWEOS) (small symbol +) and SCOZA (small symbol ×) for the λ values used in this work. The lines serve as a guide for the eye. Symbols show the simulation data of del Río *et al.* (□) (Ref. 1), Vega *et al.* (◇) (Ref. 52), de Miguel (▽) (Ref. 53), Orkoulas and Panagiotopoulos (◁) (Ref. 9), Elliot and Hu (△) (Ref. 51), and Pagan and Gunton (▷) (Ref. 55).

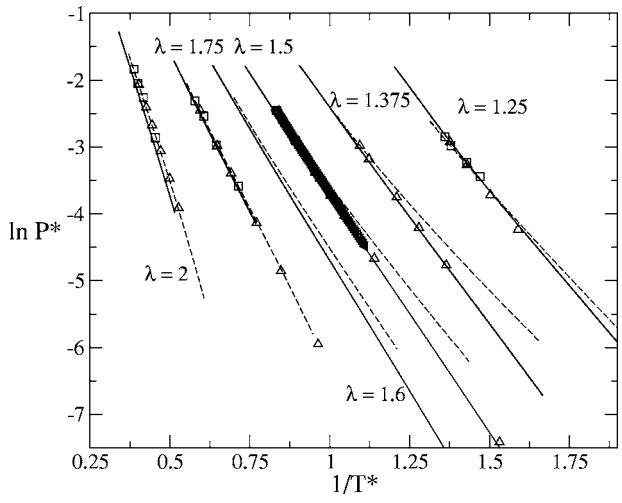

FIG. 6. Clausius-Clapeyron representation of the saturated pressure as a function of the range of the potential, $1.25 \leqslant \lambda \leqslant 2$. The solid and dashed lines are perturbation theory (IRSWEOS and LRSWEOS) and SCOZA for the λ values used in this work. Symbols show the simulation data of del Río *et al.* (□) (Ref. 1), Orkoulas and Panagiotopoulos (◁) (Ref. 9), and Elliot and Hu (△) (Ref. 51).

triangles △); for decreasing λ we find a rather flat region ($\lambda \in [2.3,3]$), then a decreasing of ρ_c^* followed by a rapidly increasing ρ_c^* if one moves further to smaller interaction ranges. Although the critical points for the region $2<\lambda<3$ have not yet been explored by simulations, SCOZA and LRSWEOS allow us to visualize the behavior of the reduced critical density in this region. Both approaches converge basically to the same value at $\lambda=3$ that was obtained by Orkoulas and Panagiotopoulos.

Figures 6 and 7 show the Clausius-Clapeyron representation of the saturated pressure for all λ values considered in this work. It is obvious from Fig. 6, that for intermediate ranges SCOZA and IRSWEOS yield a good description of the saturated pressure when compared with simulation data. However, we observe a deviation between the approaches when $\lambda \leqslant 1.6$, where IRSWEOS gives a better description especially for low temperatures (see the simulation data for $\lambda=1.5$). For long ranges, as shown in Fig. 7, the agreement between both theoretical approaches is very good for the whole temperature range. In particular, there are no differences between theories and simulation data for the case $\lambda=3$.

Figure 8 describes the behavior of the reduced critical pressure P_c^* as a function of the SW range. This figure illustrates that the IRSWEOS and LRSWEOS tend to overestimate P_c^* for all λ values. Nevertheless, the SCOZA is in

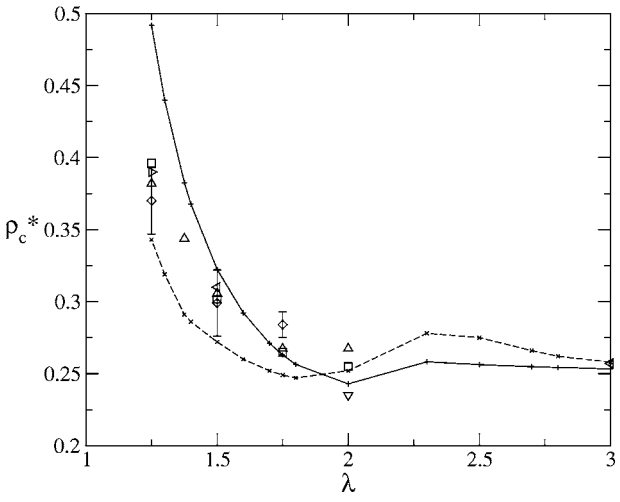

FIG. 5. Critical density as a function of the range of the potential, λ. The solid and dashed lines are interpolations between critical densities predicted by both perturbation theory (IRSWEOS and LRSWEOS) and SCOZA for the λ values used in this work. The lines serve as a guide for the eye. Symbols show the simulation data of del Río *et al.* (□) (Ref. 1), Vega *et al.* (◇) (Ref. 52), de Miguel (▽) (Ref. 53), Pagan and Gunton (▷) (Ref. 55), Elliot and Hu (△) (Ref. 51), and Orkoulas and Panagiotopoulos (◁) (Ref. 9).

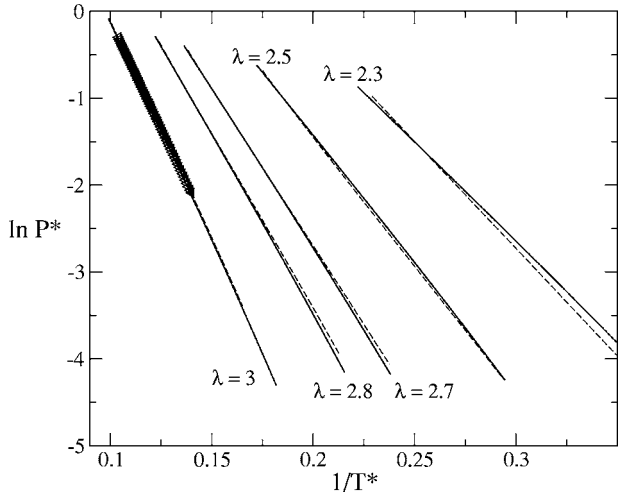

FIG. 7. Clausius-Clapeyron representation of the saturated pressure as a function of the range of the potential, $2<\lambda\leqslant 3$. The solid and dashed lines are perturbation theory (LRSWEOS) and SCOZA results for the λ values used in this work. Symbols show the simulation data of Orkoulas and Panagiotopoulos (◁) (Ref. 9).

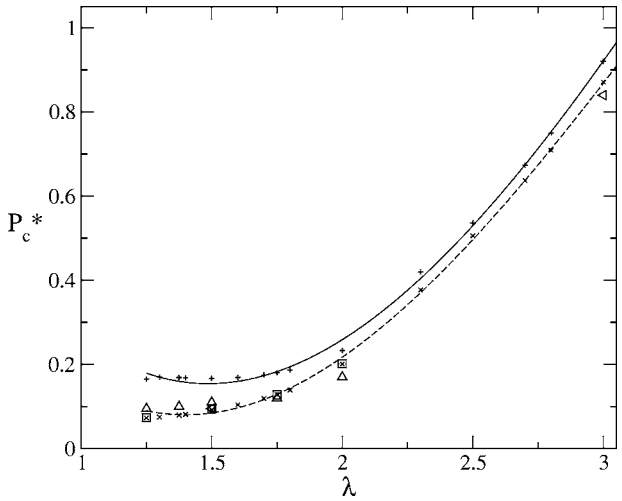

FIG. 8. Critical pressure as a function of the range of the potential, λ. The solid and dashed lines are polynomial fits to the critical pressures predicted by both perturbation theory (IRSWEOS and LRSWEOS) (small symbols +) and SCOZA (small symbols ×) for the λ values used in this work. The lines serve as a guide for the eye. Symbols show the simulation data of del Río *et al.* (□) (Ref. 1), Elliot and Hu (△) (Ref. 51), and Orkoulas and Panagiotopoulos (◁) (Ref. 9).

excellent agreement with the simulation data. Based on the SCOZA results, we also propose an analytical expression for the reduced critical pressure as a function of the interaction range $\lambda: P_c^*(\lambda)=0.155+0.326\lambda-0.705\lambda^2+0.385\lambda^3-0.053\lambda^4$. The critical-point parameters T_c^*, ρ_c^*, and P_c^* obtained within SCOZA and the IRSWEOS and LRSWEOS are summarized in Table I. The T_c^* values given therein can be compared with simulation data and other theoretical results listed in Table I and Table II of Ref. 8. We have not included the data of Vega *et al.*[52] in Fig. 6 and 8 since their saturated pressures show an error between 10% and 20% and the slope exhibits an unphysical behavior when λ is varied (see also the discussion by Elliott and Hu[51] and del Río *et al.*[1]).

A comparison with simulation data has shown that the accuracy of SCOZA deteriorates with decreasing interaction range. In this context we have investigated the sensitivity of the numerical solution of the SCOZA PDE with regard to the choice of the density ρ_0, which is the value of the density where the high-density boundary condition of Eq. (13) is placed. For the long-ranged SW fluid we found that the solution is rather insensitive to the choice of ρ_0. For example, for $\lambda=3$ and $\rho_0^*=0.8$, 0.9, 1, 1.1, and 1.2 the resulting coexistence curves are practically indistinguishable on the scale of the figures. However, with decreasing interaction range λ we observed that we had to move ρ_0 to larger densities in order to obtain SCOZA results that are insensitive to a further increase of ρ_0. On the other hand, the possibility of moving ρ_0 to larger densities is limited by the fact that the LMV algorithm no longer converges for very high densities and low temperatures. As a compromise we have chosen $\rho_0^*=1.15$ for the shorter-ranged cases. The error of the SCOZA solution due to the influence of the high-density boundary condition amplifies if one goes down to lower and lower temperatures when solving the SCOZA PDE. So, while the critical-point temperature T_c^* is still precisely predicted also for the short ranged SW fluids the accuracy of the liquid side of the coexistence curve deteriorates (see, e.g., the SCOZA coexistence curve for $\lambda=1.5$ of Fig. 1). This deterioration of the SCOZA for short-ranged SW fluids might be due to the fact that the only assumption made by the SCOZA, namely, that the direct correlation function is of the same range as the interaction potential, is no longer suitable for very short-ranged potentials. These difficulties are also encountered with other liquid-state theories, such as the MSA or the ORPA, which are known to fail for very narrow attractive potentials. In order to improve the performance of the ORPA for narrow attractive wells Pini *et al.*[56] have developed a modified version of the ORPA, which they called nonlinear ORPA, since the contributions to the direct correlation function are nonlinear in the interaction potential. Taking into account a functional form of the direct correlation

TABLE I. Critical-point parameters T_c^*, ρ_c^*, and P_c^* for different values of λ obtained from SCOZA and IRSWEOS and LRSWEOS.

	SCOZA			IRSWEOS and LRSWEOS		
λ	T_c^*	ρ_c^*	P_c^*	T_c^*	ρ_c^*	P_c^*
3	9.941	0.258	0.871	10.089 9	0.253 3	0.920 6
2.8	8.069	0.262	0.709	8.187 8	0.254 3	0.750 2
2.7	7.230	0.266	0.637	7.333 1	0.254 8	0.673 6
2.5	5.712	0.275	0.506	5.805 2	0.256 3	0.536 5
2.3	4.366	0.278	0.377	4.504 4	0.258 2	0.419 7
2	2.699	0.252	0.201	2.785 1	0.242 9	0.232 9
1.8	1.957	0.247	0.139	2.089 5	0.256 4	0.186 7
1.75	1.809	0.249	0.128	1.948 4	0.263 0	0.180 1
1.7	1.672	0.252	0.119	1.817 1	0.271 0	0.175 1
1.6	1.427	0.260	0.104	1.577 6	0.292 2	0.168 8
1.5	1.210	0.272	0.092	1.360 3	0.322 4	0.166 7
1.4	1.014	0.286	0.081	1.155 5	0.367 7	0.168 1
1.375	0.978	0.291	0.079	1.104 8	0.382 6	0.168 8
1.3	0.843	0.319	0.075	0.948 5	0.439 8	0.170 0
1.25	0.761	0.343	0.073	0.831 9	0.491 7	0.165 4

function similar to that considered in the nonlinear ORPA might also improve the SCOZA for short-ranged interactions and is left to future work.

IV. CONCLUSIONS

We have used the self-consistent Ornstein-Zernike approximation (SCOZA) and analytical equations of state based on a perturbation theory (IRSWEOS and LRSWEOS) to determine the liquid-vapor phase diagram of the square-well fluid of variable interaction range. In general, both approaches describe quantitatively the vapor-liquid phase diagram of the square-well fluid when compared with simulation data.

We have shown that SCOZA yields very precise predictions for the binodal curves especially for the case of long-ranged SW systems ($\lambda \geqslant 1.75$). Furthermore, the analytical equations of state are able to describe the binodal curves and the saturated pressures for the whole range of λ values considered if one stays away from the critical region. It is well known that the prediction of the critical points by means of the standard statistical mechanics techniques such as perturbation theories, integral equation theories, or density-functional theories is a difficult task. However, we have shown in the present work that SCOZA gives accurate estimates for the critical thermodynamic variables for all the λ values considered. In particular, for $\lambda \geqslant 1.5$, the predictions for the critical temperatures and the critical pressures agree with the simulation results to about 5%. This has allowed us to present analytical expressions for the critical temperatures and pressures as functions of λ. In all cases considered, the analytical equations of state tend to overestimate these critical-point parameters. For the critical density we observed a larger dispersion of both simulation data and theoretical approaches. When comparing the theoretical approaches with simulation data for $\lambda > 2$ we noticed an erratic behavior of the simulation data[10,28] in the liquid branch, suggesting that additional more refined simulations are required.

Due to the success of SCOZA in describing the critical region, further analysis will be considered in future work. Finally, we conclude that this work allows us to identify the regions of applicability of both frameworks, at least for the SW fluid of variable interaction range. We find that both approaches complement each other and they are efficient methods that can be used in a great variety of applications.

ACKNOWLEDGMENTS

This work was supported by the Österreichische Forschungsfond under Project No. P15758. One of the authors (E.S.-P.) gratefully acknowledges discussions with J. Köfinger and G. Kahl. The other two (A.L.B.) and (R.C.-P.) acknowledge support from PROMEP (SEP, México) and CONACYT (Grants No. 41678-F, and No. 46373/A-1).

[1] F. del Río, E. Avalos, R. Espíndola, L. F. Rull, G. Jackson, and S. Lago, Mol. Phys. **100**, 2531 (2002).
[2] F. del Río and L. Lira, J. Chem. Phys. **87**, 7179 (1987).
[3] J. Largo, J. R. Solana, S. B. Yuste, and A. Santos, J. Chem. Phys. **122**, 084510 (2005) and references therein.
[4] P. Bolhuis, M. Hagen, and D. Frenkel, Phys. Rev. E **50**, 4880 (1994).
[5] C. Rascón, G. Navascués, and L. Mederos, Phys. Rev. B **51**, 14899 (1995).
[6] G. Foffi, G. D. McCullagh, A. Lawlor, E. Zaccarelli, K. Dawson, F. Sciortino, P. Tartaglia, D. Pini, and G. Stell, Phys. Rev. E **65**, 031407 (2002).
[7] J. F. Lutsko, and G. Nicolis, J. Chem. Phys. **122**, 244907 (2005).
[8] A. Reiner and G. Kahl, J. Chem. Phys. **117**, 4925 (2002).
[9] G. Orkoulas and A. Z. Panagiotopoulos, J. Chem. Phys. **110**, 1581 (1999).
[10] B. H. Patel, H. Docherty, S. Varga, A. Galindo, and G. C. Maitland, Mol. Phys. **103**, 129 (2005).
[11] Y. H. Fu and S. I. Sandler, Ind. Eng. Chem. Res. **34**, 1897 (1995).
[12] J. Chang and S. I. Sandler, Mol. Phys. **81**, 745 (1994).
[13] P. D. Fleming III and R. J. Brugman, AIChE J. **33**, 729 (1987).
[14] A. Gil-Villegas, A. Galindo, P. J. Whitehead, S. J. Mills, G. Jackson, and A. N. Burgess, J. Chem. Phys. **106**, 4168 (1997).
[15] A. L. Benavides and F. del Río, Mol. Phys. **68**, 983 (1989).
[16] A. Gil-Villegas, F. del Río, and A. L. Benavides, Fluid Phase Equilib. **119**, 97 (1996).
[17] R. Dickman and G. Stell, Phys. Rev. Lett. **77**, 996 (1996).
[18] D. Pini, G. Stell, and N. B. Wilding, Mol. Phys. **95**, 483 (1998).
[19] E. Schöll-Paschinger, D. Levesque, J.-J. Weis, and G. Kahl, J. Chem. Phys. **122**, 024507 (2005).
[20] E. Schöll-Paschinger and G. Kahl, J. Chem. Phys. **123**, 134508 (2005).
[21] E. Schöll-Paschinger, J. Chem. Phys. **120**, 11698 (2004).
[22] A. L. Benavides and A. Gil-Villegas, Mol. Phys. **97**, 1225 (1999).
[23] A. L. Benavides, Y. Guevara, and D. del Río, Physica A **202**, 420 (1994).
[24] A. L. Benavides, Y. Guevara, and A. F. Estrada-Alexanders, J. Chem. Thermodyn. **32**, 420 (2000).
[25] Y. Guevara, A. L. Benavides, A. F. Estrada-Alexanders, and M. Romero, J. Phys. Chem. B **104**, 7490 (2000).
[26] A. L. Benavides and Y. Guevara, J. Phys. Chem. B **107**, 9477 (2003).
[27] A. Vidales, A. L. Benavides, and A. Gil-Villegas, Mol. Phys. **99**, 703 (2001).
[28] A. L. Benavides, F. del Río, and J. Alejandre, Mol. Phys. **74**, 321 (1991).
[29] J. S. Høye and G. Stell, J. Chem. Phys. **67**, 439 (1977).
[30] J. S. Høye and G. Stell, Mol. Phys. **52**, 1071 (1984).
[31] D. Pini, G. Stell, and R. Dickman, Phys. Rev. E **57**, 2862 (1998).
[32] A. Borge and J. S. Høye, J. Chem. Phys. **108**, 4516 (1998); J. S. Høye and A. Borge, *ibid.* **108**, 8830 (1998); N. U. Andresen, A. Borge, and J. S. Høye, *ibid.* **115**, 9165 (2001).
[33] S. Grollau, Ph. D. thesis, Université Pierre et Marie Curie, 2001; S. Grollau, E. Kierlik, M.-L. Rosinberg, and G. Tarjus, Phys. Rev. E **63**, 041111 (2001); S. Grollau, M.-L. Rosinberg, and G. Tarjus, Physica A **296**, 460 (2001).
[34] J. S. Høye and G. Stell, Physica A **244**, 176 (1997); **247**, 497 (1997); D. Pini, J. S. Høye, and G. Stell, *ibid.* **307**, 469 (2002).
[35] A. G. Dickman and G. Stell, Mol. Phys. **100**, 3021 (2002).
[36] C.-L. Lee and G. Stell, J. Phys.: Condens. Matter **14**, 4815 (2002).
[37] D. Pini, G. Stell, and J. S. Høye, Int. J. Thermophys. **19**, 561 (1998).
[38] D. Pini, G. Stell, and N. B. Wilding, J. Chem. Phys. **115**, 2702 (2001).
[39] G. Kahl, E. Schöll-Paschinger, and G. Stell, J. Phys.: Condens. Matter **14**, 9153 (2002).
[40] E. Schöll-Paschinger and G. Kahl, Europhys. Lett. **63**, 538 (2003).
[41] E. Schöll-Paschinger and G. Kahl, J. Chem. Phys. **118**, 7414 (2003).
[42] J. S. Høye, D. Pini, and G. Stell, Physica A **279**, 213 (2000).
[43] E. Waisman, Mol. Phys. **25**, 45 (1973).
[44] G. Stell, J. Chem. Phys. **55**, 1485 (1971).
[45] H. C. Andersen and D. Chandler, J. Chem. Phys. **57**, 1918 (1972).
[46] J. P. Hansen and I. R. McDonald, *Theory of Simple Liquids*, 2nd ed. (Academic, New York, 1986).
[47] S. Labik, A. Malijevsky, and P. Vonka, Mol. Phys. **56**, 709 (1985).
[48] N. F. Carnahan and K. E. Starling, J. Chem. Phys. **51**, 635 (1969)
[49] J. A. Barker and D. Henderson, J. Chem. Phys. **47**, 2856 (1967); **47**, 4714 (1967).

[50] In this work we have used old and recent computer simulation data. In our analysis we have taken into account that most of the new data have improved (Refs. 1 and 10).
[51] J. R. Elliott and L. Hu, J. Chem. Phys. **110**, 3043 (1999).
[52] L. Vega, E. de Miguel, L. F. Rull, G. Jackson, and I. A. McLure, J. Chem. Phys. **96**, 2296 (1992).
[53] E. de Miguel, Phys. Rev. E **55**, 1347 (1997).
[54] A. Galindo (private communication).
[55] D. L. Pagan and J. D. Gunton, J. Chem. Phys. **122**, 184515 (2005).
[56] D. Pini, A. Parola, and L. Reatto, Mol. Phys. **100**, 1507 (2002).